Spatial and Temporal Patterns and Drivers of Grassland NEP in the Muri Region, 2000 to 2022

Suju Meng[1], Peng Wang[2], Wenping Yin[2], Botao He[2], Pei Li[2] and Yong Xue[2,3]

[1]Natural Resources Comprehensive Investigation and Monitoring Institute of Qinghai Province, Xining, Qinghai Province, China. [2]School of Environment and Spatial Informatics, China University of Mining and Technology, Xuzhou, Jiangsu Province, China. [3]College of Engineering and Technology, University of Derby, Derby, UK.

Air, Soil and Water Research
Volume 17: 1–10

DOI: 10.1177/11786221241271557

ABSTRACT: The Muri region of Qinghai Province is not only the source of important water sources, but also one of the key areas targeted by the ecological environment restoration project. The study of the Net ecosystem productivity (NEP) of grassland in the Muri region is of great importance in order to gain insight into the health of grassland ecosystems and to assess the carbon sink capacity. In this study, the net primary productivity (NPP) and NEP of the grassland in the Muri region from 2000 to 2022 were calculated using remote sensing data, meteorological data and land cover data, coupled with Carnegie-Ames-Stanford Approach (CASA) model and soil heterotrophic respiration model. The spatial and temporal patterns of NEP of grassland ecosystems over different periods from 2000 to 2022 were assessed following accuracy tests. The drivers affecting the spatial and temporal changes in NEP of grasslands in the Muri region were then explored with the help of Geogdetector. The study indicated that: (1) From 2000 to 2022, the mean annual NEP of grassland in the Muri region was 138.23 gC/m^2, exhibiting a significant increasing trend ($p < 0.01$). (2) Spatially, the NEP of grassland showed a pattern of distribution from south-east to north-west, from the center to either side and from high to low values, with 91.58% of grassland showing an increasing trend in all growth periods. (3) Climatic factors, altitude and slope are important drivers of changes in the NEP of grassland, with altitude being the most important factor influencing the NEP of grassland in this region. This study can provide valuable references for assessing the carbon sequestration capacity of grassland ecosystems and monitoring the health of grassland ecosystems in the Muri region, as well as for formulating future ecological protection policies and directions in the Muri region.

KEYWORDS: Muri region, net ecosystem productivity, spatio-temporal variations, remote sensing

RECEIVED: January 25, 2024. **ACCEPTED:** June 12, 2024.

TYPE: Original Research

CORRESPONDING AUTHOR: Yong Xue, China University of Mining and Technology School of Environment Science and Spatial Informatics, Xuzhou 221116, China. Email: yx9@hotmail.com

Introduction

Amidst the global climate change scenario, studying the carbon cycle process and carbon sequestration potential of terrestrial ecosystems can shed light on the vegetation's ability to absorb atmospheric carbon dioxide, and also provide insights into the quality of terrestrial ecology. Additionally, it holds immense significance for comprehending the state of terrestrial ecosystems' carbon sinks and regional carbon balance (Baker et al., 2018; Friend et al., 2013; Schimel et al., 2014; Yan et al., 2023). Grassland ecosystems constitute a vital element of the terrestrial biosphere and represent one of the most significant carbon reservoirs and absorbers on land (C. B. Chen; He et al., 2015; Li & Peng, 2022; Vourlitis et al., 2022).

Net Ecosystem Productivity (NEP), calculated by subtracting soil heterotrophic respiration (R_h) from Net Primary Productivity (NPP), is a reliable measure of carbon sequestration and emission capacity, and is often used to determine whether a region is a carbon source or sink (Fang et al., 2001). NEP can accurately depict the carbon sequestration capability of the area. As a crucial factor in grassland health, this variable characterizes the activity of herbaceous plants and has a significant impact on the carbon sinks and ecological processes of grassland ecosystems. As the important indicator of grassland ecosystem growth and health, it also serves as an important ecological indicator for the sustainable development of ecosystems (Liang et al., 2022; Lu et al., 2023; Peichl et al., 2013; Zhou et al., 2018). To estimate NEP, NPP and soil heterotrophic respiration must first be estimated. The advancement of remote sensing technology has led to the incorporation of remote sensing data in NPP estimation models. These models, namely climate productivity models (Veroustraete et al., 1994), light energy utilization models (C. B. Chen, Li, & Peng, 2022; Liang et al., 2022; Zhu et al., 2007), and ecosystem process models (Field et al., 1995; He et al., 2015, Nkrumah et al., 2022), have effectively addressed the limitations of traditional NPP estimation methods, which were time-consuming and restricted to small-scale estimates. As such, they are now the primary approach to NPP estimation. Among these models, the Carnegie-Ames-Stanford Approach (CASA) model has emerged as a leading approach for estimating NPP due to its notable advantages, including straightforward access to input data, simplicity of implementation, and rapid speed of large-scale NPP estimation. It has been extensively employed for both global and regional estimation of NPP (Cramer et al., 1999, Na et al., 2013; Wu et al., 2022; M. L. Zhang et al., 2020).

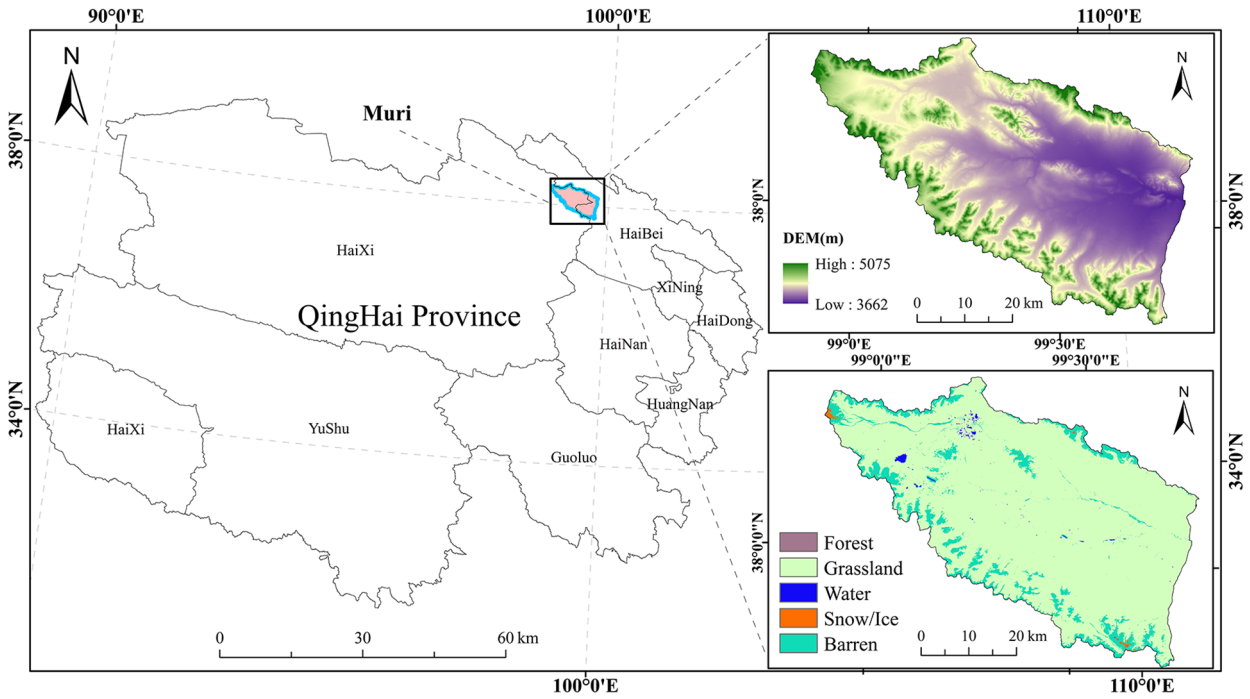

Figure 1. Geography of the Muri region.

The Muri region is significant as the origin of the Datong River, which is a crucial tributary of the upper reaches of the Yellow River. Additionally, it forms an essential component of the water source and ecological security barrier of the Qilian Mountain region, holding a critical ecological status. In recent years, China has undertaken ecological restoration initiatives in nearby mining regions and established monitoring schemes for alpine grasslands (Qian et al., 2017, 2020). However, there is currently a lack of clarity regarding the health of the region's grasslands in recent years, their capacity for carbon sequestration, and the relationship between climate and other influences. Furthermore, few studies have focused on the region. Accurately estimating NEP of grassland ecosystems in the region and analyzing their spatial and temporal changes and driving forces can enhance understanding of the carbon sequestration potential and quality status of local grassland ecosystems. This information is of great theoretical and practical value for monitoring and replanting projects.

In this paper, Landsat remote sensing imagery and meteorological data were used to estimate the NPP and NEP of the Muri region from 2000 to 2022 by coupling the CASA model and soil respiration estimation model. Then we utilized trend analysis and Geogdetector to observe the changes in NEP during each growth period of the grassland, investigated the features of temporal and spatial variations as well as the factors that stimulate these changes. The results aim to provide scientific references for research concerned with the dynamics of grass ecosystem functioning and monitoring the health status of grasslands in the Muri region.

Materials and Methods

Study area

The Muri region is situated in Haixi Mongol and Tibetan Autonomous Prefecture, as well as Haibei Tibetan Autonomous Prefecture in Qinghai Province. It can be found at the headwaters of the Datong River system, with an administrative area that spans the three counties of Tianjun, Gangcha, and Qilian. This region also includes the Muri Mining Area and a portion of the Qinghai Area located in the southern foothills of the Qilian Mountains. The total area covered by this region is 2,453 km^2. 56 km^2, located between longitude 98°53′ to 99°47′ East and latitude 37°49′ to 38°19′ North.

As shown in Figure 1, the Muri region has typical alpine climatic characteristics, with an average altitude of 4,000 m, a high terrain distribution in the north-west and a low terrain distribution in the south-east, and is mainly dominated by the plateau ice-marginal landform type. A surface area of 9.8% in the Muri region comprises shrubland, while the remainder (89.6%) is grassland. Dominant in this latter category are plants that can withstand low temperatures and droughts, with low levels of vegetation, dense grasses and inconspicuous hierarchical differentiation. However, the community structure is relatively simple, and the ability to resist disturbance is weak (Qian et al., 2020).

Data source

Acquisition of NDVI. As detailed in Table 1, the Landsat image dataset was used as the primary source of remote sensing

Table 1. Landsat Image Time Series.

TIME	DATA PRODUCTS	SPATIAL RESOLUTION (M)
2000–2011	USGS Landsat 5 Level 2, Collection 2, Tier 1	30
2012	USGS Landsat 7 Level 2, Collection 2, Tier 1	30
2013–2022	HLS Operational Land Imager Surface Reflectance and TOA Brightness Daily Global	30
2020–2022	HLS Sentinel-2 Multi-spectral Instrument Surface Reflectance Daily Global	30

imagery in this study. The Normalized Vegetation Index (NDVI) was calculated using the red and near-infrared bands. It is important to note that NDVI refers to the Normalized Vegetation Index throughout the study.

Meteorological data. The meteorological data include monthly mean temperature, monthly total precipitation and monthly total solar radiation for the period 2000 to 2022, the monthly mean temperature and monthly total precipitation are from the National Oceanic and Atmospheric Administration (NOAA) National Centers for Environmental Information (NCEI; https://www.ncei.noaa.gov/maps/daily/), obtained by collating meteorological data, and the monthly total solar radiation is from the NOAA NCEP-DOE Reanalysis 2 dataset (https://psl.noaa.gov/data/gridded/data.ncep.reanalysis2.html).

Land cover data. The land cover data used in this study are from the 30 m China Land Cover dataset (http://www.ncdc.ac.cn) and ESRI 10 m land cover data (https://livingatlas.arcgis.com/landcover/) for the time periods 2000 to 2020 and 2021 to 2022, respectively. For the period 2000 to 2022, grassland distribution data for the Muri region were extracted year by year. The data was resampled for the years 2021 to 2022 with a uniform spatial resolution of 30 m.

Data validation. In the absence of directly measured data, we validated our findings using cross-comparison of multiple data. The multiple data consisted of the MODIS NPP product (MOD17A3H v006), available at (http://ladsweb.modaps.eosdis.nasa.gov/), the actual NPP of the Tibetan Plateau grasslands, the Potential Net Primary Productivity and the Potential Aboveground Biomass datasets from 2000 to 2018, available at (https://doi.org/10.11888/Ecolo.tpdc.271204). MOD17A3H is an NPP data product made available by NASA EOS/MODIS. It is chiefly used in NPP studies at different spatial levels and is only accessible on an annual basis (D. Li & Wang, 2018). The second dataset was similarly calculated using the CASA model in order to obtain. In addition, the calculation results of other researchers were also taken into account.

Estimation of NPP

In this study, the improved CASA model was used to simulate the NPP in the Muri region. The model utilizes remote sensing data as input data, combining environmental variables (temperature, moisture, and soil) and vegetation physiological parameters. It then represents NPP as the product of APAR and light energy utilization. The specific formula for the calculation is as follows:

$$NPP(x,t) = APAR(x,t) \times \varepsilon(x,t) \quad (1)$$

Where the APAR(x,t) is the photosynthetically active radiation absorbed by image x in month t (MJ/m^2/month); $\varepsilon(x,t)$ is the actual light energy use of image x in month t (gC/MJ). NPP(x,t) is the net primary productivity (NPP) of the vegetation at location x at time t (gC/m^2/month).

APAR absorbed by vegetation can be expressed in terms of total solar radiation and the fraction of photosynthetically active radiation (FPAR). The expression of APAR is as follows:

$$APAR(x,t) = \frac{1}{2} \times SOL(x,t) \times FPAR(x,t) \quad (2)$$

Where: SOL(x,t) represents the overall solar radiation at pixel x during month t (MJ/m^2 /month); FPAR(x,t) indicates the proportion of incident photosynthetically active radiation that the vegetation layer absorbs (unitless); and the fixed value of 0.5 indicates the proportion of solar active radiation (with wavelengths varying between 0.38 and 0.71 μm) that can be used by vegetation in comparison to the total solar radiation.

$\varepsilon(x,t)$ represents the efficiency of green vegetation in absorbing light energy and converting it into organic carbon over a given time period. This value represents another crucial parameter for estimating NPP. It is influenced by a number of factors, including temperature, humidity and the maximum light energy utilization (ε_{max}) in the actual environment. The expression of $\varepsilon(x,t)$ is as follows:

$$\varepsilon(x,t) = T_1(x,t) \times T_2(x,t) \times W_\varepsilon(x,t) \times \varepsilon_{max} \quad (3)$$

Where: $\varepsilon(x,t)$ denotes the actual light energy use efficiency of image x in month t (gC/MJ). Since the light energy use efficiency is in reality affected by many external environmental factors, mainly temperature and precipitation, that is, the temperature factors $T_1(x,t)$ and $T_2(x,t)$, the specific formula can be referred to the model established by other researchers (Field et al., 1995). $W_\varepsilon(x,t)$ is the moisture stress factor. ε_{max} (gC/MJ) is the maximum light energy use of vegetation in the ideal state. In this study, the maximum light energy efficiency of grassland was 0.542 gC/MJ.

Estimation of soil respiration

The soil respiration estimation model employed in this study was derived from the regression equation of temperature, precipitation, and carbon emission based on the relationship between carbon emission and environmental factors in the Wudaoliang experimental site in Qinghai Province. The model was applied in this paper to estimate the distribution of soil microbial respiration within the alpine steppe area of the Muri region. The following calculation formula was utilized:

$$R_h = 0.22 \times \left(Exp\left(0.0913 \times T\right) + Ln\left(0.3145 \times R + 1\right)\right) \times 30 \times 46.5\% \quad (4)$$

Where R_h is the heterotrophic respiratory consumption (gC/m²/month); T is the average monthly air temperature (°C); and R is the total monthly precipitation (mm).

Estimation of NEP

NEP is the fraction of NPP minus the consumption of photosynthetic products by heterotrophic respiration (soil respiration), that is:

$$NEP = NPP - \mathrm{R_h} \quad (5)$$

where NEP is net ecosystem productivity (gC/m²/month), NPP is net primary productivity (gC/m²/month), and R_h is heterotrophic respiration consumption (gC/m²/month).

Trend analysis

In this study, the trend analysis of annual NEP of grassland in Muri region from 2000 to 2022 was carried out by using the Theil-Sen Median method, which is computationally efficient, insensitive to measurement errors and leptokurtic data, and suitable for trend analysis of long time series data (J. L. Chen, Shao, et al., 2022; Rong & Long, 2021). Its calculation formula is:

$$\beta = \mathrm{Median}\left(\frac{\mathrm{x_j} - \mathrm{x_i}}{\mathrm{j} - \mathrm{i}}\right) \forall\, \mathrm{j} > i \quad (6)$$

In the formula, the function Median() represents the calculation of the median value. A value of $\beta > 0$ denotes an increasing trend in the data, while a value of $\beta < 0$ indicates a decreasing trend.

To assess the significance of the results, the Mann-Kendall (MK) test is employed. This non-parametric test allows the detection of trends in time series, irrespective of the distribution of the data and the presence of missing values or outliers. It is particularly suitable for the analysis of long-term trends (Kamali et al., 2020; Rong & Long, 2021). The formula for the MK test is shown below:

$$\mathrm{S} = \sum_{\mathrm{i=1}}^{\mathrm{n-1}} \sum_{\mathrm{j=i+1}}^{\mathrm{n}} \mathrm{sgn}\left(\mathrm{x_j} - \mathrm{x_i}\right) \quad (7)$$

$$\mathrm{sgn}\left(\mathrm{x_j} - \mathrm{x_i}\right) = \begin{cases} +1 \mathrm{x_j} - \mathrm{x_i} > 0 \\ 0 \mathrm{x_j} - \mathrm{x_i} = 0 \\ -1 \mathrm{x_j} - \mathrm{x_i} < 0 \end{cases} \quad (8)$$

$$\mathrm{Z} = \begin{cases} \dfrac{\mathrm{S}}{\sqrt{\mathrm{Var(S)}}} (\mathrm{S} > 0) \\ 0 (\mathrm{S} = 0) \\ \dfrac{\mathrm{S}+1}{\sqrt{\mathrm{Var(S)}}} (\mathrm{S} < 0) \end{cases} \quad (9)$$

$$\mathrm{Var(S)} = \frac{\mathrm{n(n-1)(2n+5)}}{18} \quad (10)$$

where S and Z are test statistics, n is the amount of data in the sequence.

The significance test is also a bilateral trend test, where the critical value $Z_1 - \alpha/2$ is found in the normal distribution table at a given level of significance; when $|Z| \leq Z_1 - \alpha/2$, the original hypothesis is accepted, that is, the trend is not significant; and if $|Z| > Z_1 - \alpha/2$, the original hypothesis is rejected, that is, the trend is considered to be significant. The trend is considered significant. In this paper, given the significance level $\alpha = 0.05$, the critical value $Z_1 - \alpha/2 = \pm 1.96$, when the absolute value of Z is greater than 1.65, 1.96, and 2.58, it means that the trend passes the significance test with a confidence level of 90%, 95%, and 99%, respectively. The method of determining the significance of the trend is shown in Table 2.

Geogdetector

Geogdetector is a statistical method for studying the patterns of spatial differentiation of geographical elements and revealing the driving factors behind them (Wang et al., 2022). The Geogdetector consists of four parts: the factor probe, the interaction probe, the risk probe, and the ecological probe.

The factor detector is premised on the notion that if an independent variable x has a consequential impact on a dependent variable y, then the spatial distributions of variables x and y will display a marked spatial similarity. The correlation between x and y may be quantified by the q statistic. The formula is as follows:

$$\mathrm{q} = 1 - \frac{\sum_{\mathrm{h=1}}^{\mathrm{L}} \mathrm{N_h} \sigma^2{}_{\mathrm{h}}}{\mathrm{N}\sigma^2} \quad (11)$$

Table 2. Mann-Kendall Test Trend Categories.

β	Z	TREND TYPE	TREND FEATURES
$\beta > 0$	$2.58 < Z$	4	Extremely significant increase
	$1.96 < Z \leqslant 2.58$	3	Significant increase
	$1.65 < Z \leqslant 1.96$	2	Slightly significant increase
	$Z \leqslant 1.65$	1	Insignificant increase
$\beta = 0$	Z	0	No change
$\beta < 0$	$Z \leqslant 1.65$	−1	Insignificant decrease
	$1.65 < Z \leqslant 1.96$	−2	Slightly significant decrease
	$1.96 < Z \leqslant 2.58$	−3	Significant decrease
	$2.58 < Z$	−4	Extremely significant decrease

Table 3. Types of Driver Interactions.

TYPE OF INTERACTION	INTERACTIVE RELATIONSHIP
Nonlinear weakening	$q(X1 \cap X2) < \text{Min}[q(X1), q(X2)]$
Single-factor nonlinear weakening	$\text{Min}[q(X1), q(X2)] < -q(X1 \cap X2) < \text{Max}[q(X1), q(X2)]$
Bi-factor enhancement	$q(X1 \cap X2) > \text{Max}[q(X1), q(X2)]$
Independent	$q(X1 \cap X2) = q(X1) + q(X2)$
Nonlinear enhancement	$q(X1 \cap X2) > q(X1) + q(X2)$

Where: $h = 1,2 \ldots L$ is the classification of the independent variable x; N_h and N are the sample sizes of the hth level and the whole, respectively. $\sigma^2{}_h$ and σ^2 are the variance of the dependent variable y of the hth level and the whole, respectively. q is in the range of 0 to 1, and the larger the value of q is, the greater the degree of explanation of the independent variable x on the dependent variable y, and vice versa, the smaller the value of q is.

Interaction detectors can ascertain the extent to which two drivers' explanatory power is influenced, increased, reduced, or unaffected by examining the q-statistics of the two independent factors, $X1$ ($q(X1)$), $X2$ ($q(X2)$), and the $X1$ and $X2$ interaction ($q(X1 \cap X2)$). Details of the interaction types are given in Table 3.

Results and Discussion

NPP estimation results and validation

In this study, the NPP values calculated for each month were further processed to give the annual average NPP and then compared with MOD17A3H. In order to enhance the reliability of the results of this experiment, the results of this experiment are compared and analyzed with the results of other scholars who have also adopted the improved CASA model, due to the remote sensing images are covered by clouds and other reasons, so the remote sensing images of the Muri region time series are some months, some areas of the missing data, in order to complete the comparison of annual data, the twelve months of data are complete and the entire region missing part of the year for the comparison of verification.

As shown in Table 4, this study's calculations align with the MOD17A3H data product and findings from other scholars using the same model. The reasons for the discrepancy may be as follows:

(1) The spatial resolution of the MOD17A3H product is 500 m, while the results of this study are 30 m. It is possible that the discrepancy between the two may be attributed to the spatial heterogeneity. Furthermore, the MOD17A3H is derived from the sum of all 8-day Net Photosynthesis (PSN) products (MOD17A2H) from the given year. The PSN value is the difference of the Gross Primary Productivity (GPP) and the Maintenance Respiration (MR). In contrast to the CASA model, which represents NPP directly, the fraction consumed to maintain respiration is already eliminated in the inversion of maximum light energy utilization. The calculation of the two results is distinct, the sources of uncertainty are disparate, and the results will be disparate as well.

(2) The CASA model is widely used because of its simple input parameters and easy access to data, but the different forms of input data also introduce uncertainty, which causes some differences between the calculation results of this study and the results obtained by other scholars using the same model.

Spatial distribution of annual NEP results

Due to the lack of NEP measurement data, it was not possible to verify NEP, but this experiment cross-checked the NPP estimation results and referred to other scholars' estimation results of grassland productivity in Qinghai, for the grassland in this study, the NPP and NEP estimation results were in the range of reasonably similar values. In addition, the CASA model has been extensively applied in various regions and ecosystems, demonstrating its effectiveness. Thus, the NEP estimation results presented in this study are reliable in terms of spatial and temporal changes. The detection of significant features and patterns of change enables an accurate reflection of the grassland situation in the Muri region. Figure 2 displays the annual NEP averages' spatial distribution within the Murray region between 2000 and 2022.

Table 4. Comparison of Calculations Based on the Improved CASA Model.

YEARS	IMPROVED CASA MODEL (GC/M²/YEAR)	MOD17A3H (GC/M²/YEAR)	PERCENTAGE DEVIATION (%)	OTHER DATA RESULTS (GC/M²/YEAR)	PERCENTAGE DEVIATION (%)
2003	134.84	138.22	2.51	151.54	11.02
2004	205.13	151.38	11.08	175.15	2.80
2005	166.09	168.65	1.54	170.48	2.57
2006	149.15	172.65	15.76	166.28	10.30
2010	220.84	192.23	12.95	204.67	7.90
2011	135.86	158.43	16.61	161.45	15.85
2014	217.80	152.03	30.20	180.91	20.39
2015	108.32	145.72	3.22	165.26	8.89
2016	195.39	189.72	2.90	197.90	1.27
2017	160.50	173.80	8.28	191.51	16.19
Average	169.39	164.28	3.01	176.51	4.20

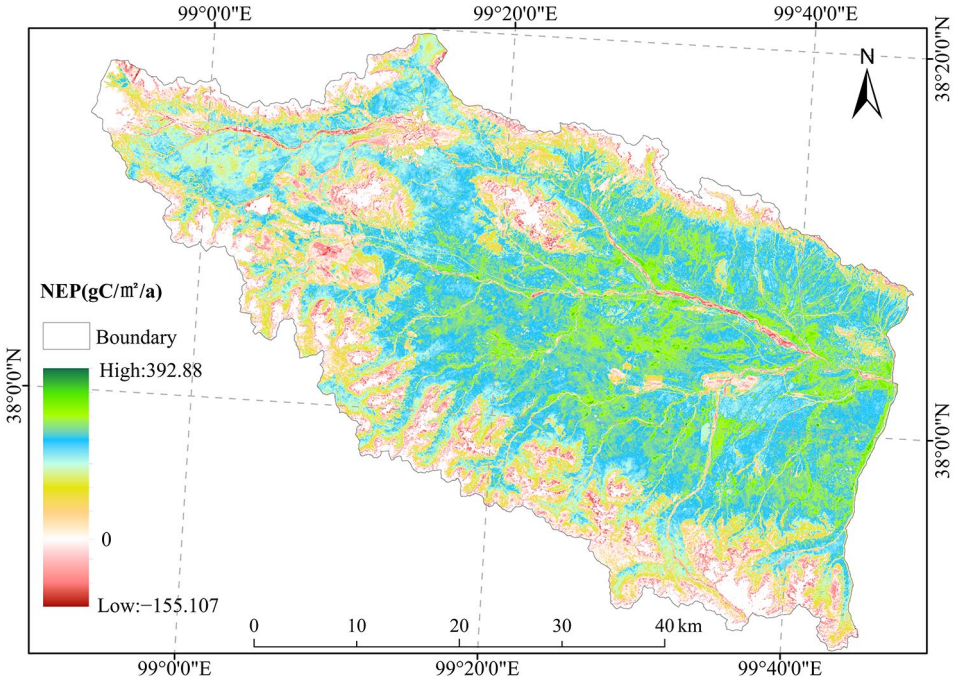

Figure 2. Spatial distribution of the 23-year average NEP in the Muri region.

The Muri region is oriented in a northwest-southeast direction, and its NEP displays a spatial distribution pattern from south-east to north-west, from the center to both sides, from high values to low values. The spatial pattern is determined by the topography of the Muri region, as illustrated in Figure 1. The elevation of the Muri region is high in the north-west and low in the south-east. Furthermore, the elevation of the south-eastern region is gradually decreasing from the two sides to the middle. The lower the elevation, the greater the temperature. As the temperature rises, the rate of grass photosynthesis and carbon fixation increases. This is particularly evident in the north-western region, where the elevation is high and the climate is characterized by low temperatures, prolonged periods of ice and snow cover, and high levels of cloud cover (Cano et al., 2023). These climatic conditions result in reduced rates of grass photosynthesis and carbon fixation. Between 2000 and 2022, the overall average NEP of grassland in the study area was 138.23 gC/m², indicating a better carbon sink status. However, areas with carbon source status are mainly located in high-elevation areas with perennial snow, bare ground areas

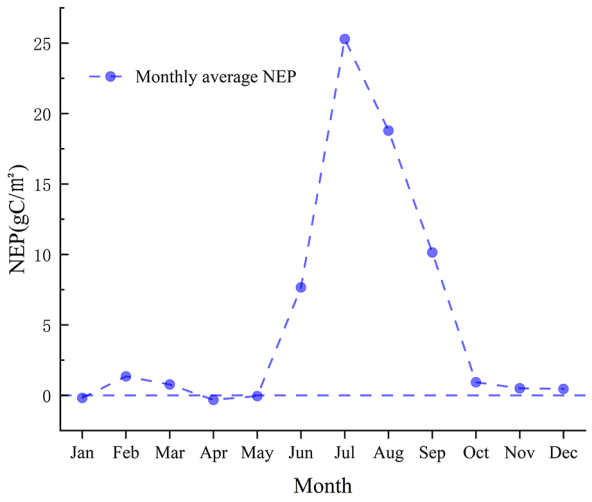

Figure 3. Monthly average NEP change curve.

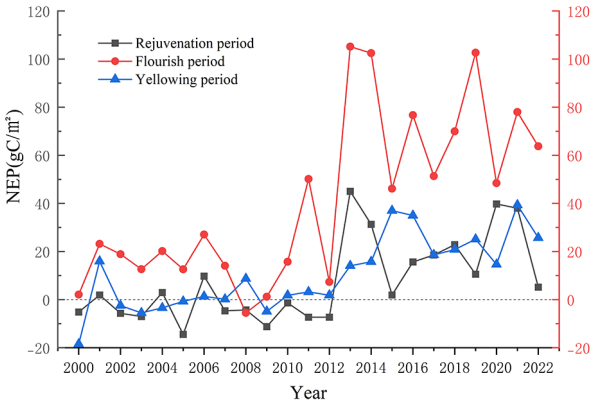

Figure 4. Changes in NEP of grassland by growth period in Muri region, 2000–2022.

due to the destruction of grasslands, or river areas experiencing occasional droughts and broken streams.

Temporal changes in NEP

Figure 3 depicts the monthly fluctuations of the mean NEP in the Muri area, ranging between −0.18 and 25.28 gC/m^2. The highest value (25.28 gC/m^2) occurred in July. The May to October timeframe displayed greater variation, indicating a carbon sink. The remaining months demonstrated weaker carbon sources or carbon sinks, fluctuating above and below 0.

In order to objectively reflect temporal changes in the NEP of grassland, this study starts from the growing season of grassland, which is divided into three periods, the rejuvenation period (May–June), the flowering period (July–August) and the yellowing period (September–October), to study the temporal change rule. As illustrated in the Figure 4, from 2000 to 2022, the NEP of grassland in the three periods showed a trend of slow growth, which means that the carbon sink capacity of grassland in the Muri region is slowly increasing. Among them, the rejuvenation and yellowing periods gradually changed from a state of fluctuating weak carbon sinks/sources to a clearly observable carbon sink state. Additionally, the carbon sink capacity during the flourishing period significantly increased. These changes indicate that the carbon absorption capacity of the grassland has been strengthened, resulting in an increase in the amount of carbon fixed.

Analysis of trends

The aforementioned results suggest that the grassland in the Muri region is developing positively. To demonstrate this change, the current study examined and performed a significance test on the trend of the grassland's annual NEP and the three growing periods from the year 2000 to 2022 in the Muri region. The results are presented in Figure 5.

As depicted in Figure 5(a), 91.58% of the grassland in Muri region show an increasing trend, of which 81.71% exhibit a non-significant increase, while the marginal, significant, and highly significant increases are 6.68%, 8.65%, and 2.96%, respectively. This suggests that the carbon absorption capability of grassland in the region has slowly improved during the period of 2000 to 2022. Moreover, it reflects that the status of grassland growth is steadily improving over time. From Figure 5(b)–(d), it is evident that the carbon sequestration capacity of grassland in the Muri region was enhanced to varying degrees in all growth periods. The geographical distribution of the areas showing a significant or highly significant increase during the rejuvenation period closely matched the direction of the rivers in the Muri region, suggesting that moisture played a crucial role in the increase of the carbon sequestration capacity of grassland during the rejuvenation period. Conversely, areas with less moisture exhibited a non-significant increase in the carbon sequestration capacity status. The trend of grassland in the Muri region during the period of flourishing and yellowing was similar, with most areas exhibiting a significant or highly significant upward trend, while some areas displayed a non-significant or significant or even highly significant downward trend during the three periods. Combined with past years' land cover data, it can be observed that most of these areas are located on the periphery of bare land or have transformed into bare land. This indicates that the local grassland has suffered varying degrees of damage or degradation (Qian et al., 2017, 2020), resulting in a significant reduction in carbon sequestration capacity.

Driving factors for NEP

Factor detection. In this study, a unidirectional detection analysis of NEP and five prospective determinants was carried out at different intervals of the grass growing season in the Muri locality. The results are shown in Figure 6.

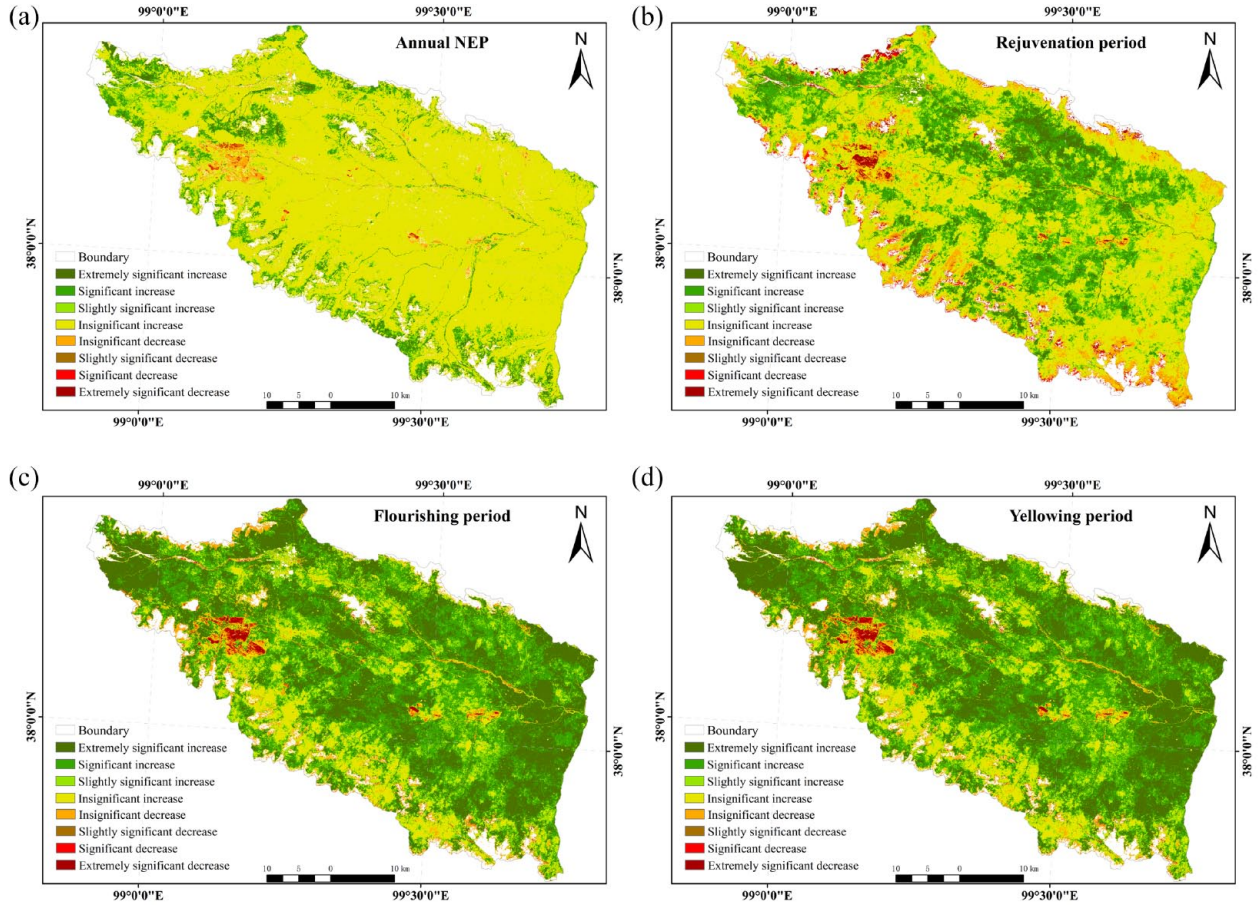

Figure 5. (a) Trends in annual NEP, (b) trends in NEP during the rejuvenation period, (c) trends in NEP during the flourishing period, and (d) trends in NEP during the yellowing period.

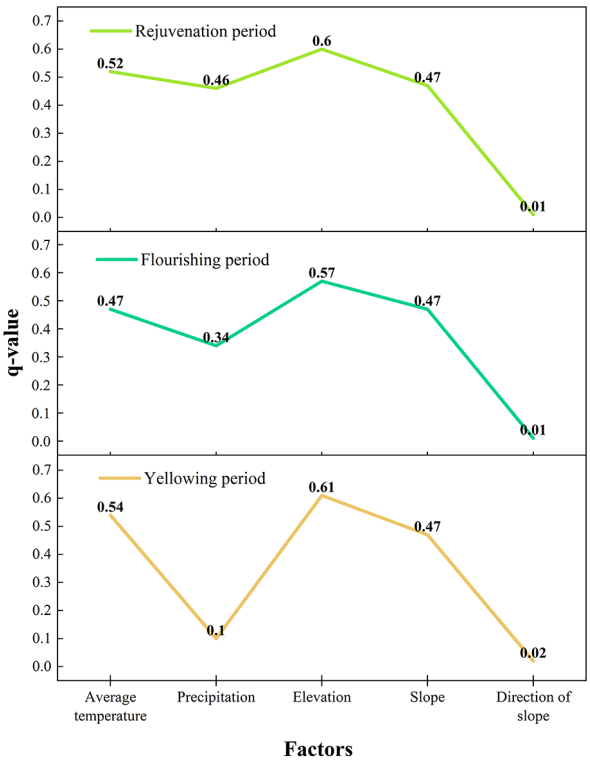

Figure 6. Results of single-factor detection at different periods of the growing season.

The p-value for each factor was 0, thus signifying that the importance of each specific factor was significant. During various periods throughout the grass growing season, the *q*-values of elevation attained maximum values of 0.60, 0.57, and 0.61, which clearly illustrates that the elevation distribution had the most influential role in explaining the differences in the spatial distribution of NEP. Direction of slope exhibited the lowest explanatory ability for variances in NEP's spatial distribution, portraying *q*-values of 0.01, 0.01, and 0.02, respectively. During the rejuvenation period, the impact of various factors demonstrated a hierarchy with elevation having the greatest influence, followed by mean temperature, slope, precipitation, and direction of slope. In contrast, the influence of variables during the flourishing period ranked elevation as the most impactful, followed by slope and mean temperature, then precipitation and direction of slope. Finally, in the yellowing period, the hierarchy remained largely unchanged with elevation, mean temperature, slope, precipitation, and direction of slope respectively demonstrating the greatest impact.

From merging the outcomes of the experiments and the discoveries made by other researchers (X. J. Li et al., 2023; Mao et al., 2014; Yan et al., 2023; L. X. Zhang et al., 2019; M. L. Zhang et al., 2020; Zhou et al., 2018), the subsequent trends can be condensed. (1) During various stages of grass growth, both temperature and precipitation directly impact grass NEP

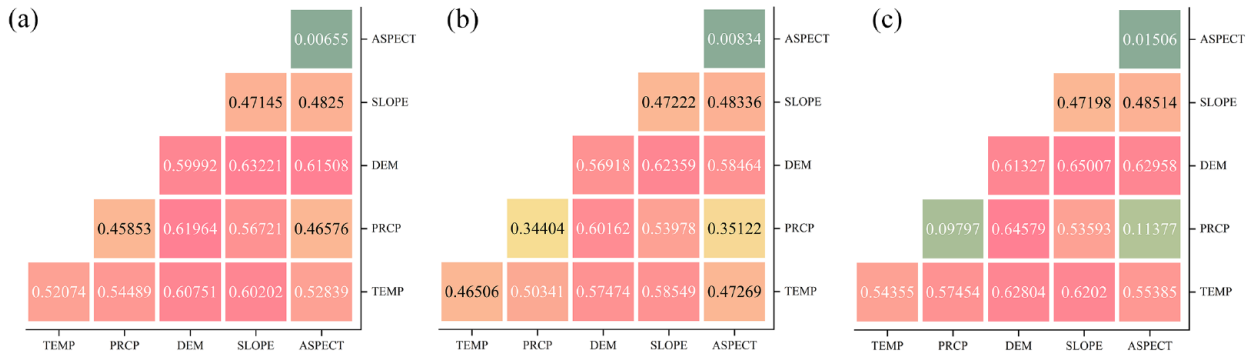

Figure 7. (a) Interaction of factors during rejuvenation period, (b) interaction of factors during flourishing period, and (c) interaction of factors during yellowing period.

through their effect on photosynthetic activity, the length of the growing season, and the intensity of soil respiration. It is important to note the impact of external factors as they have a significant effect on the overall grass growth process. (2) Slope affects grass NEP differently by influencing water uptake, land fertility distribution, exposure to sunlight, and temperature. Moreover, as the altitude increases, the climate becomes colder and the high mountain areas are covered with snow and ice all year round, which limits the growth of grasses through severe soil erosion, mainly by freeze-thaw erosion.

Factor interaction analysis. Interaction detection of factors at different times through geodetector. As shown in Figure 7. The interaction between any two drivers had a greater impact on NEP than the independent effect of a singular factor. This reveals either a two-factor enhancement or a non-linear enhancement effect. During all three stages of the growing season, the q-values of the four-factor interactions, namely temperature, precipitation, elevation, and slope, were consistently high. Furthermore, the interactions of elevation with each of the aforementioned factors were the highest among all three seasons, implying that elevation is the primary factor that influences NEP in grasslands. Temperature, precipitation, and slope are also important factors affecting NEP in grassland ecosystems. Furthermore, variations in elevation and slope result in fluctuations in temperature and precipitation, ultimately influencing the NEP of grassland ecosystems. This influence is due to a combination of climatic and topographical factors.

Conclusions

In this study, we used remote sensing images, meteorological data and land cover data, combined with physiological and ecological parameters of vegetation, to estimate NPP in Muri region using CASA model, coupled with heterotrophic respiration model to further obtain NEP. It should be noted that the estimation results of this study are subject to some uncertainty. For instance, the maximum light energy utilization of grassland assumed by the model may not be applicable to alpine grassland. Additionally, there will be some uncertainty in the production process of the input data. Furthermore, the lack of universality of some empirical formulas will lead to some unavoidable errors in the estimation results. Currently, the resolution of NPP standard products is up to 500 m. The spatial heterogeneity of different resolutions and the scarcity of ground stations make it challenging to obtain ground data, which in turn makes data validation difficult. Furthermore, it is even more challenging to directly validate NEP results.

We analyzed the spatial and temporal changes in NEP in the Muri region between 2000 and 2022. From 2000 to 2022, the mean annual NEP of grassland in the Muri region was 138.23 gC/m^2, exhibiting a significant increasing trend ($p < .01$). Spatially, the NEP of grassland showed a pattern of distribution from south-east to north-west, from the center to either side and from high to low values, with 91.58% of grassland showing an increasing trend in all growth periods. Most of the areas that experienced a decreasing trend underwent a process of changing from grassland to bare ground and back again during the period, like the mining process in the Muri coal field. The restoration of mining and grassland ecosystems will be the primary focus of future ecological protection in the Muri region. Concurrently, it is imperative to reduce the damage to alpine grassland ecosystems caused by human activities. (3) Climatic factors, altitude, and slope are important drivers of changes in the NEP of grassland, with altitude being the most important factor influencing the NEP of grassland in this region. This research serves as a benchmark for tracking grassland ecosystem carbon sequestration capability and health in the Muri area, the results demonstrated that the grassland ecosystems in the region had exhibited a relatively healthy state over the past few decades. This was evidenced by a general trend of increasing carbon fixation in all periods of the growing season. This indicated that the amount of carbon fixed into the ecosystems eventually increases during the growing season of the grasslands.

Finally, it is recommended that further detailed and in-depth studies be conducted in the future to elucidate the interconnections between photosynthesis and respiration in alpine grassland ecosystems and the influences of climate and topography. Such studies will facilitate a comprehensive

understanding of these relationships, which will in turn assist in the elucidation of the processes of carbon cycling in these fragile ecosystems. Furthermore, these results will contribute to the management of ecosystem resources and their environment.

Declaration of conflicting interests

The author(s) declared no potential conflicts of interest with respect to the research, authorship, and/or publication of this article.

Funding

The author(s) disclosed receipt of the following financial support for the research, authorship, and/or publication of this article: This work was supported in part by the National Natural Science Foundation of China (NSFC) under Grant No. 42275147.

REFERENCES

Baker, H. S., Millar, R. J., Karoly, D. J., Beyerle, U., Guillod, B. P., Mitchell, D. M., Shiogama, H., Sparrow, S. N., Woollings, T., & Allen, M. R. (2018). Higher CO_2 concentrations increase extreme event risk in a 1.5°C world. *Nature Climate Change*, 8, 604–608.

Cano, D., Crispin, A., Custodio, M., Chanamé, F., Peñaloza, R., & Pizarro, S. (2023). Space-time quantification of aboveground net primary productivity service supply capacity in high Andean bofedales using remote sensors. *Journal of Water and Land Development*, 15(21), 15472.

Chen, C. B., Li, G. Y., & Peng, J. (2022). Spatial and temporal analysis of NPP of natural grassland in Xinjiang in the last 20 years. *Geography of Arid Zones*, 42(2), 522–534.

Chen, J. L., Shao, Z. F., Huang, X., Zhuang, Q. W., Dang, C. Y., Cai, B. W., Zheng, X. K., & Ding, Q. (2022). Assessing the impact of drought-land cover change on global vegetation greenness and productivity. *Science of the Total Environment*, 852, 158499.

Cramer, W., Kicklighter, D. W., Bondeau, A., Iii, B. M., Churkina, G., Nemry, B., Ruimy, A., & Schloss, A. L., & Intercomparison TPOTPNM. (1999). Comparing global models of terrestrial net primary productivity (NPP): Overview and key results. *Global Change Biology*, *5*(S1), 1–15.

Fang, J. Y., Ke, J. H., Tang, Z. Y., & Chen, A. P. (2001). The concept, estimation and interrelationship of the "4Ps" of biological productivity. *Journal of Plant Ecology*, 25(4), 414–419.

Field, C. B., Randerson, J. T., & Malmstrom, C. M. (1995). Global net primary production: Combining ecology and remote sensing. *Remote Sensing of Environment*, 51, 74–88.

Friend, A. D., Lucht, W., Rademacher, T. T., Keribin, R., Betts, R. A., Cadule, P., Ciais, P., Clark, D. B., Dankers, R., Falloon, P., Ito, A., Kahana, R., Kleidon, A., Lomas, M. R., Nishina, K., Ostberg, S., Pavlick, R. P., Peylin, P., Schaphoff, S., Vuichard, N., Warszawski, L., Wiltshire, A., & Woodward, F. I. (2013). Carbon residence time dominates uncertainty in terrestrial vegetation responses to future climate and atmospheric CO_2. *Proceedings of the National Academy of Sciences*, 111, 3280–3285.

He, Y. H., Ma, Z. H., & Guo, X. L. (2015). Grassland productivity simulation: Integrating remote sensing and an ecosystem process model. In L. Jonathan & X. J. Yang (Eds.), *Monitoring and modeling of global changes: A geomatics perspective*. Springer Netherlands (pp. 155–169).

Kamali, A., Khosravi, M., & Hamidianpour, M. (2020). Spatial–temporal analysis of net primary production (NPP) and its relationship with climatic factors in Iran. *Environmental Monitoring and Assessment*, 192, 1–20.

Li, D., & Wang, Z. (2018). The characteristics of NPP of terrestrial vegetation in China based on MOD17A3 data. *Ecology and Environmental Sciences*, 27, 397–405.

Li, X. J., Li, R. R., & Sha, Z. Y. (2023). Modeling carbon uptake by vegetation of grassland ecosystems and its associated factors in China based on remote sensing. *Frontiers in Earth Science*, 10, 1077885.

Liang, L., Geng, D., Yan, J., Qiu, S. Y., Shi, Y. Y., Wang, S. G., Wang, L. J., Zhang, L. P., & Kang, J. R. (2022). Remote sensing estimation and spatiotemporal pattern analysis of terrestrial net ecosystem productivity in China. *Remote Sensing*, 14, 1902.

Lu, X. J., Chen, Y., Sun, Y. Y., Xu, Y. M., Xin, Y., & Mo, Y. P. (2023). Spatial and temporal variations of net ecosystem productivity in Xinjiang Autonomous Region, China based on remote sensing. *Frontiers in Plant Science*, 14, 1146388.

Mao, D. H., Wang, Z. M., Li, L., & Ma, W. H. (2014). Spatiotemporal dynamics of grassland aboveground net primary productivity and its association with climatic pattern and changes in Northern China. *Ecological Indicators*, 41, 40–48.

Na, S. I., Hong, S. Y., Kim, Y. H., Lee, K. D., & Jang, S. Y. (2013). Prediction of rice yield in Korea using paddy rice NPP index-Application of MODIS data and CASA model. *Korean Journal of Remote Sensing*, 29(5), 461–476.

Nkrumah, T., Meiling, Z., Stephen, N., & Xingyu, W. (2022). Response of carbon budget to climate change of the alpine meadow in Gannan using the CENTURY model. *Journal of Water and Climate Change*, 13(6), 2298–2318.

Peichl, M., Sonnentag, O., Wohlfahrt, G., Flanagan, L. B., Baldocchi, D. D., Kiely, G., Galvagno, M., Gianelle, D., Marcolla, B., & Pio, C. (2013). Convergence of potential net ecosystem production among contrasting C3 grasslands. *Ecology Letters*, 16(4), 502–512.

Qian, D. W., Yan, C. Z., Xing, Z. P., & Xiu, L. N. (2017). Monitoring coal mine changes and their impact on landscape patterns in an alpine region: A case study of the Muli coal mine in the Qinghai-Tibet Plateau. *Environmental Monitoring and Assessment*, 189, 1–13.

Qian, D. W., Yan, C. Z., & Xiu, L. N. (2020). Vulnerability response of land cover changes and landscape patterns in and around the muri mining area on the Tibetan plateau. *Journal of Glaciology and Geocryology*, 42(4), 1134–1343.

Rong, T., & Long, L. H. (2021). Quantitative assessment of NPP changes in the yellow river source area from 2001 to 2017 [Conference session]. IOP Conference Series: Earth and Environmental Science, IOP Publishing.

Schimel, D. S., Stephens, B. B., & Fisher, J. B. (2014). Effect of increasing CO_2 on the terrestrial carbon cycle. *Proceedings of the National Academy of Sciences of the United States of America*, 112, 436–441.

Verburg, P. S., Arnone, J. A. III, Obrist, D., Schorran, D. E., Evans, R. D., Leroux-Swarthout, D., Johnson, D. W., Luo, Y., & Coleman, J. S. (2004). Net ecosystem carbon exchange in two experimental grassland ecosystems. *Global Change Biology*, 10(4), 498–508.

Veroustraete, F., Patyn, J., & Myneni, R. B. (1994). *Forcing of a simple ecosystem model with fAPAR and climatic data to estimate regional scale photosynthetic assimilation*. In F. Veroustraete , R. J. M. Ceulemans, I. I. P. Impens, & J. Van Rensbergen (Eds.), *Vegetation, modelling and climatic change effects* (pp. 151–177). Academic Publishing.

Vourlitis, G. L., Pinto, O. B. Jr., Dalmagro, H. J., Enrique Zanella de Arruda, P., de Almeida Lobo, F., & de Souza Nogueira, J. (2022). Net primary production and ecosystem carbon flux of Brazilian tropical savanna ecosystems from eddy covariance and inventory methods. *Journal of Geophysical Research: Biogeosciences*, 127(8), e2021JG006780.

Wang, H., Liu, Y. X., Cai, L. P., Fan, D. J., Wang, Y. J., & Yao, Y. (2022). Regional differentiation in the ecological effects of land cover change in China. *Land Degradation & Development*, 33(2), 346–357.

Wu, C. Y., Chen, K. L., You, X. N., He, D. C., Hu, L. B., Liu, B. K., Wang, R. K., Shi, Y. Y., Li, C. X., & Liu, F. M. (2022). Improved CASA model based on satellite remote sensing data: Simulating net primary productivity of Qinghai Lake Basin alpine grassland. *Geoscientific Model Development*, 15(17), 6919–6933.

Yan, Z. Y., Gao, Z. H., Sun, B., Ding, X. Y., Gao, T., & Li, Y. F. (2023). Global degradation trends of grassland and their driving factors since 2000. *International Journal of Digital Earth*, 16, 1661–1684.

Zhang, L. X., Zhou, D. C., Fan, J. W., Guo, Q., Chen, S. P., Wang, R. H., & Li, Y. Z. (2019). Contrasting the performance of eight satellite-based GPP models in water-limited and temperature-limited grassland ecosystems. *Remote Sensing*, 11, 1333.

Zhang, M. L., Liu, X. N., Nazieh, S., Wang, X. Y., Nkrumah, T., & Hong, S. L. (2020). Spatiotemporal distribution of grassland NPP in Gansu province, China from 1982 to 2011 and its impact factors. *PLOS ONE*, 15(11), e0242609.

Zhou, W., Yang, H., Zhou, L., Chen, Y., Huang, L., & Ju, W. (2018). Dynamics of grassland carbon sequestration and its coupling relation with hydrothermal factor of Inner Mongolia. *Ecological Indicators*, 95, 1–11.

Zhu, W. Q., Pan, Y. Z., & Zhang, J. S. (2007). Remote sensing estimation of net primary productivity of terrestrial vegetation in China. *Journal of Plant Ecology*, 31(3), 413–424.